ChemPubSoc Europe

DOI: 10.1002/ejic.201600278

EurJIC European Journal of Inorganic Chemistry

Full Paper

Photoreactive Ru Complexes

Highly DNA-Photoreactive Ruthenium 1,4,5,8-Tetraazaphenanthrene Complex Conjugated to the TAT Peptide: Efficient Vectorization inside HeLa Cells without Phototoxicity – The Importance of Cellular Distribution

Lionel Marcélis,[a] Sofia Kajouj,[a] Jonathan Ghesquière,[a] Gregory Fettweis,[b] Isabelle Coupienne,[b] Rémy Lartia,[c] Mathieu Surin,[d] Eric Defrancq,[c] Jacques Piette,[b] Cécile Moucheron,[a] and Andrée Kirsch-De Mesmaeker*[a]

Dedicated to the memory of Ivo Nnganyadi[‡]

Abstract: The photoreactive $[Ru(TAP)_2(phen)]^{2+}$ (TAP = 1,4,5,8-tetraazaphenanthrene; phen = 1,10-phenanthroline) complex tethered to the cell-penetrating peptide (CPP) TAT was studied in vitro and in cellulo. The tethering of the complex does not affect its behavior under blue-light irradiation in the presence of guanine-containing oligodeoxyribonucleotides (ODN_G). Thus, the luminescence is quenched in the presence of ODN_G, and gel electrophoresis experiments showed the appearance of products corresponding to the irreversible attachment of the conjugate to ODN_G upon illumination. The cellular uptake of the conjugate was examined by flow cytometry, inductively coupled plasma mass spectrometry (ICP-MS), and confocal imaging microscopy. These experiments showed that the $[Ru(TAP)_2(phen\text{-}TAT)]$ conjugate is readily taken up by HeLa cells and, despite these favorable factors, the cellular survival was 100 %, as measured by a 3-(4,5-dimethylthiazol-2-yl)-2,5-diphenyltetrazolium bromide (MTT) assay. A possible origin of the inactivity of $[Ru(TAP)_2(phen\text{-}TAT)]$ under irradiation is proposed on the basis of the fluorescence-activated cell sorting (FACS), ICP-MS, and confocal microscopy results.

Introduction

For many years, ruthenium(II) polypyridyl complexes have received a lot of attention thanks to their interactions with DNA, especially intercalation inside the base-pair stack.[1–3] This increased interest is also due to the photoinduced reactivity of these complexes with the guanine bases of DNA.[4,5] A simple change of ligand coordinated to the metal center allows the properties of the resulting complex to be tailored and, thereby, enables its interaction and photoreactivity with DNA to be tuned. When the extensively studied dipyrido[3,2-*a*;2′,3′-*c*]phenazine (dppz) ligand[1] or other large planar ligands such as 1,10-phenanthrolino[5,6-*b*]1,4,5,8,9,12-hexaazatriphenylene (PHEHAT)[2] and tetrapyrido[3,2-*a*:2′,3′-*c*:3′′,2-*h*:2′′,3-*j*]acridine (tpac)[6] are chelated to Ru^{II} centers [in combination with two other 2,2′-bipyridine (bpy) or 1,10-phenanthroline (phen) spectator ligands], the resulting complexes behave as DNA intercalators. Most of these have been examined as DNA photoprobes because their luminescence, quenched in water, is switched on in the presence of DNA.[7] In contrast, the use of highly π-deficient ligands such as 1,4,5,8-tetraazaphenanthrene (TAP) or 1,4,5,8,9,12-hexaazatriphenylene (HAT) enhances the photo-oxidizing power of the resulting complex, so that a photoinduced electron transfer (PET) from a guanine (G) base of DNA towards the excited complex leads to luminescence quenching.[4] Interestingly, the recombination of the two radical species generated by this PET process produces an irreversible covalent adduct between the guanine (G) moiety and the Ru^{II} complex (Figure 1, a).[8]

Owing to the interest in the study of Ru^{II} complexes in the presence of biomolecules, these metallic compounds were also examined in the presence of living cells to investigate their cellular penetration, intracellular distributions, and interactions with the different cellular components.[9,10] Most Ru^{II} polypyridyl complexes are unable to cross the membranes of living cells, as demonstrated with the standard complexes $[Ru(bpy)_3]^{2+}$, $[Ru(phen)_3]^{2+}$,[9] and some of their analogues.[11]

[a] Organic Chemistry and Photochemistry, Université libre de Bruxelles (U.L.B.),
50 Av. F. D. Roosevelt, CP160/08, 1050, Bruxelles, Belgium
E-mail: akirsch@ulb.ac.be
http://cop.ulb.ac.be/
[b] Laboratory of Virology and Immunology, GIGA-Research, University of Liège,
B34 Av. de l'Hôpital 1, Liège, 4000, Belgium
[c] Département de Chimie Moléculaire, UMR CNRS, Université Grenoble Alpes,
5250, 38000 Grenoble France
[d] Laboratory for Chemistry of Novel Materials, University of Mons - UMons,
20 Place du Parc, 7000 Mons, Belgium
[‡] A young and promising researcher who started this research project ten years ago
Supporting information and ORCID(s) from the author(s) for this article are available on the WWW under http://dx.doi.org/10.1002/ejic.201600278.

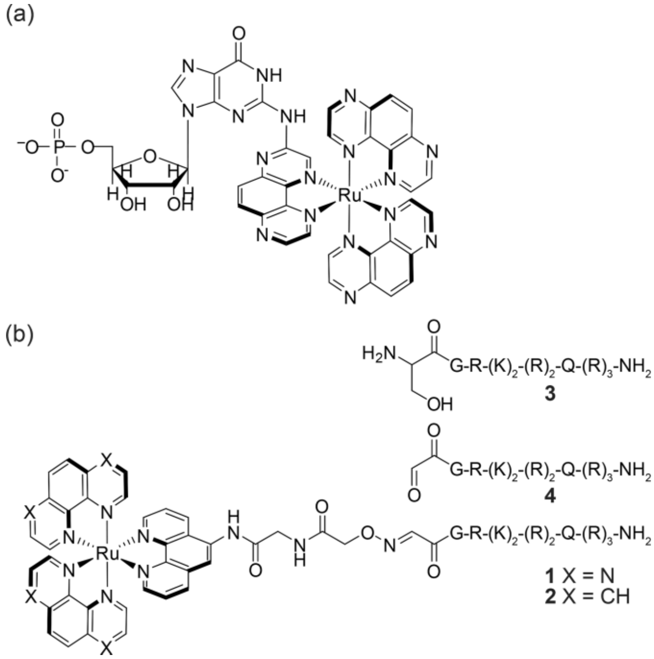

Figure 1. (a) Structure of the photoadduct obtained between a Ru–TAP complex {namely, $[Ru(TAP)_3]^{2+}$} and guanosine monophosphate (GMP). (b) Structures of the two Ru^{II}–TAT conjugates of this work: the photoreactive conjugate [Ru(TAP)$_2$(phen-TAT)] (**1**, X = N) and the photoluminescent conjugate [Ru(phen)$_2$(phen-TAT)] (**2**, X = CH). The TAT peptide with N-terminal serine **3** is oxidized to TAT–N-terminal aldehyde **4** before the reaction with complexes bearing an aminooxy function.

This penetration problem was exploited to probe cell viability through flow cytometry because, in contrast to living cells, dead cells can internalize the metallic complexes.[12] However, complexes based on the 4,7-diphenyl-1,10-phenanthroline (DIP) ligand are internalized by living cells.[9] The highly lipophilic DIP ligand enables the complex to be taken up by the cells according to a passive diffusion pathway.[13] In the same way, complexes bearing modified dppz ligands with alkyl chains are also internalized readily in the cytoplasm[14] because of their affinity for liposomal membranes.[15]

The cellular internalization of complexes can be quite different upon irradiation. Generally, Ru^{II} complexes have rather good singlet-oxygen photosensitization quantum yields,[16] which explains their capacity to alter cellular membranes.[14] Therefore, after irradiation, the cell membranes become permeable, and the Ru^{II} complex can penetrate into the cell rather easily.[11] This photoinduced internalization was demonstrated with complexes bearing modified dppz ligands. Moreover, after cell penetration, they are released from endosomes inside the cells and can then reach the nucleus.[14,17] In those cases, the light modifies the cellular distribution, which also depends on the chirality of the complexes, as has been highlighted for a dinuclear Ru^{II} complex.[18]

Strategies to enhance the uptake of metal complexes by living cells consist of tethering them to penetrating agents such as nanoparticles,[19] hormones,[20] or peptides.[21–23] Cell-penetrating peptides (CPPs) are small peptides that cross the cell membrane readily and can be attached to various cargos to deliver molecular material inside the cells.[24–26] For example, octaarginine has been attached to Ru^{II} complexes and efficiently enhanced the internalization of the tethered complexes.[23,27]

We have demonstrated that DNA-photoreactive Ru–TAP complexes conjugated to specific antisense oligonucleotides and internalized into living cells by particular synthetic polymers specifically inhibit the expression of targeted genes.[28,29] This specific photosilencing has demonstrated the efficiency of Ru–TAP complexes under irradiation inside living cells.

The goal of the present work was to use these Ru–TAP compounds to target and damage most of the DNA content of HeLa cells instead of damaging a specific DNA sequence. On the basis of previous results, this DNA photodamaging action should result in cell death[30] through a mechanism quite different from the classical oxygen photosensitization used in photodynamic therapy (PDT). Indeed, as explained above, the Ru–TAP compounds are able to photoinduce irreversible covalent binding of the TAP ligand to the G bases of DNA under visible-light irradiation (Figure 1, a).[4] However, as the naked Ru–TAP complexes cannot cross the cellular membranes, we tethered them to the TAT peptide [sequence (S)GRKKRRQRRR], which corresponds to the 48–57 sequence of the trans-activating transcriptional protein (TAT) of HIV-1.[31] The results presented in this paper are quite unexpected. Indeed, despite an excellent photoreactivity of the Ru–TAP complex tethered to the TAT peptide with in vitro G-containing DNA, this conjugate was unable to induce HeLa cell death under blue-light irradiation. This contrasts with the significant mortality caused by TAT conjugated to $[Ru(phen)_3]^{2+}$ (Figure 1, b) with the same cell internalization and irradiation conditions. The origin of this unexpected behavior for the Ru–TAP conjugate is discussed on the basis of inductively coupled plasma mass spectrometry (ICP-MS), fluorescence-activated cell sorting (FACS), and confocal microscopy results.

Results and Discussion

Tethering of Ru^{II} Complexes to TAT Peptide

Two different complexes, namely, $[Ru(TAP)_2(phen)]^{2+}$ and $[Ru(phen)_3]^{2+}$, were successfully tethered to the TAT peptide (Supporting Information, Figure SI1) through the derivatization of their phen ligands (Figure 1, b) to obtain [Ru(TAP)$_2$(phen-TAT)] (**1**) and [Ru(phen)$_2$(phen-TAT)] (**2**).[32,33] $[Ru(TAP)_2(phen)]^{2+}$ is photoreactive[4] towards the G bases of DNA and gives rise to a PET, as explained in the Introduction. In contrast, $[Ru(phen)_3]^{2+}$ is not photoreactive towards the G bases. This is the reason why the resulting conjugate **2** was used for comparison purposes (see below).

As the TAT peptide could affect the excited-state behavior of the complex and, therefore, its photoreactivity with a G base, we first examined the possible effect of the TAT attachment to $[Ru(TAP)_2(phen)]^{2+}$ upon blue-light irradiation in the absence and presence of 17-mer oligodeoxyribonucleotides (ODNs) containing no G base (ODN$_0$) or one G base (ODN$_G$) (Table 1, ODN$_G$ contains a G base at the 10th position). The best criterion of excited-state reactivity is the luminescence lifetime of the excited complex, which decreases if an electron transfer (ET) process occurs from the G base. Thus, we determined the excited-state lifetimes of **1** by time-correlated single-photon counting (TC-SPC) measurements in the absence and presence of oligonucleotide. As the quenching by the G base could be different whether it is incorporated into single-stranded (ss) or double-stranded (ds) ODN_G, both types of ODN_G were examined (Table 2). In all cases, conjugate **1** shows two lifetime components; therefore, the excited complex can sense more than one microenvironment of the peptide, the ODN, or both. For conjugate **1** in the absence of ODN, the calculated average luminescence lifetime (τ_{av}) is longer than that for the corresponding free complex $[Ru(TAP)_2(phen)]^{2+}$; therefore, the excited state is protected slightly by the TAT peptide owing to decreased radiationless deactivation by solvent molecules. This lifetime lengthening is enhanced in the presence of ODN_0, especially $dsODN_0$. In contrast, τ_{av} becomes shorter in the presence of ODN_G, and this effect is also stronger with $dsODN_G$ than with $ssODN_G$ (with $dsODN_G$, a component as short as 37 ns with a contribution of almost 60 % is observed).[34] These decreased luminescence lifetimes are a signature of quenching by PET processes with the G base of ODN_G. Thus, the data from the lifetime measurements suggest unambiguously that Ru–TAT conjugate **1** interacts with ODNs and that the photoreactivity of the complex is still efficient after it is anchored to the TAT peptide.

Table 1. Sequences of ODN duplexes used in this study.

ODN_0	5′-TAA	ATT	TAA	TAA	AAA	AA-3′
	3′-ATT	TAA	ATT	ATT	TTT	TT-5′
ODN_G	5′-TAA	ATT	TAA	GAA	AAA	AA-3′
	3′-ATT	TAA	ATT	CTT	TTT	TT-5′

Table 2. Luminescence lifetimes of excited $[Ru(TAP)_2phen]^{2+}$ and **1** in the absence and presence of ODN_0 and ODN_G (Tris/HCl 10 mM pH 7; NaCl 50 mM) under air.

	Luminescence lifetime [ns] (A_i)[a]			τ_{av} [ns][b]
$[Ru(TAP)_2phen]^{2+}$	648 (100 %)			648
1	670 (87 %)	1089 (13 %)		724
1 + $ssODN_0$	576 (50 %)	994 (50 %)		785
1 + $dsODN_0$	560 (40 %)	1609 (60 %)		1190
1 + $ssODN_G$	486 (73 %)	996 (27 %)		624
1 + $dsODN_G$	37 (58 %)	513 (25 %)	1310 (17 %)	372

[a] The luminescence decays monitored at λ = 650 nm were analyzed according to a multiexponential function: $I_{em}(t) = \Sigma_i a_i \exp(-t/\tau_i)$, ($i$ = 1, ...). The percentage contribution of the different decay components at the initial emission are shown in parentheses and were calculated according to $A_i = a_i/(\Sigma a_i)$. χ^2 was used to evaluate the quality of the fit. [b] Weighted-average luminescence lifetimes obtained according to $\tau_{av} = \Sigma a_i \tau_i / \Sigma a_i$. Experimental errors 5 %.

To get further information on the interactions between conjugate **1** and ODNs, the influence of the addition of **1** on the melting temperature (T_m) of the 17-mer ODN_G duplex was examined. The melting temperatures (Table 3) were determined by monitoring the absorbance of the solution at λ = 260 nm versus temperature. Upon the addition of increasing amounts of **1**, an increase of the melting temperature was observed; therefore, a relatively strong association between **1** and the $dsODN_G$ occurs. It should be noted that the effect is more important for the lower ionic strength (50 mM NaCl; Table 3), which indicates that the interaction is probably electrostatic.

Table 3. Melting temperatures of ODN_G duplex (2 µM) in the absence or presence of different equivalents of **1** without irradiation.

Equivalents of **1**	Melting temperature [°C] [a]
0	33 (41)
1	33 (41)
2	36 (42)
3	40 (42)

[a] The melting temperatures were determined from the absorbance at λ = 260 nm as a function of temperature. The salt concentration was either 50 or 150 mM (in parentheses) in 10 mM Tris/HCl (pH 7).

Atomistic molecular modeling was performed next on these systems through molecular dynamics (MD) simulations. The α-

(a)

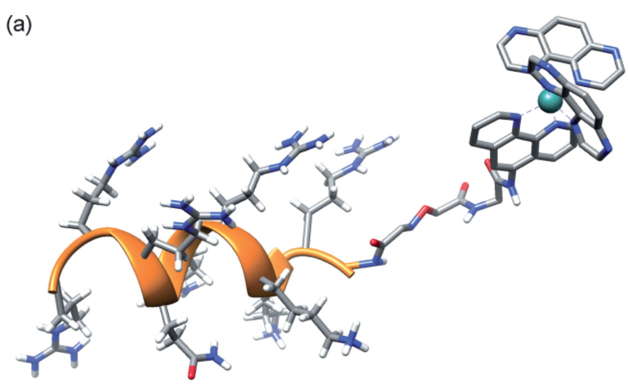

(b)

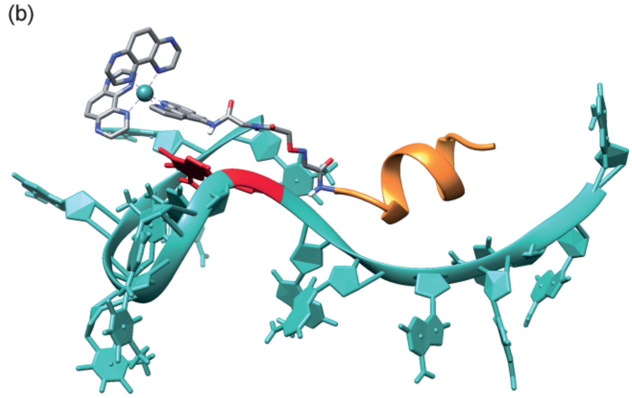

(c)

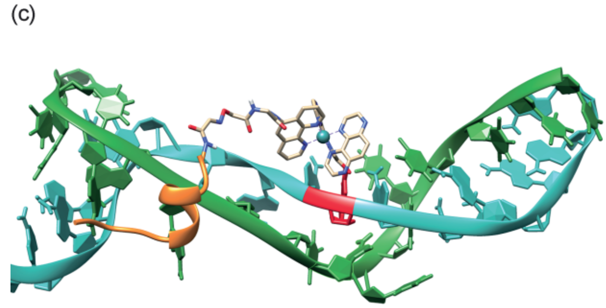

Figure 2. Molecular modeling of **1** (water molecules removed for clarity). Selected MD snapshots of (a) **1**, (b) **1** interacting with $ssODN_G$ (**1**/$ssODN_G$), and (c) the covalent binding between **1** and $dsODN_G$ (**1**-$dsODN_G$). Conjugate **1** is shown in sticks with the TAT peptide helix as an orange ribbon [for clarity, the lateral chains are only depicted in (a)]; the ODN is depicted with the backbones as a tube and the bases as blue and green rings according to the strand. For clarity, the guanine base is red.

helix geometry of **1** was found as a stable conformation in the absence of ODN, as shown in Figure 2 (a). From this geometry, MD calculations were performed on the **1**/s-ODN_G and **1**/dsODN_G systems (Figures 2, b and SI2, respectively). MD snapshots were selected for the proximity of the TAP ligands of the Ru^{II} complex with the G base of ODN (depicted in red). For the **1**/ssODN_G system, the flexible ssODN_G is folded around **1**, primarily because of the electrostatic and H-bonding interactions between the lysine (Lys) and arginine (Arg) side-chains of TAT and the phosphodiester groups of the ssODN_G. The TAT peptide remains in the α-helical conformation over the MD run; in this conformation (Figure 2, b), the nearest distance between a TAP ligand (α-carbon atom to the N atom) and the G base (amino nitrogen) is ca. 7.8 Å. For the MD simulation of the **1**/dsODN_G system, the ODN duplex remains in the B-helix conformation; the TAT part of **1** is accommodated along the major groove, and the Arg and Lys residues point towards the oxygen atoms of the phosphodiester DNA linkage. In this case, the nearest distance between a TAP ligand (α-carbon atom of the nonchelating nitrogen atom) and the G base (amino nitrogen atom) is ca. 6.3 Å. The shorter distance between the guanine and the complex for **1**/dsODN_G than for **1**/ssODN_G is in agreement with the luminescence lifetimes, for which a more significant lifetime decrease by PET is detected with dsODN_G.

Irreversible Photoadduct Formation between 1 and ODN_G

If the quenching of excited conjugate **1** by ODN_G indeed occurs through an ET process, the radicals formed by this PET can react together[4] to form a covalent bond between the TAP ligand and the G base of the ODN_G (Figure 1, a). This process should result in irreversible photo-crosslinking between **1** and ODN_G. Polyacrylamide gel electrophoresis (PAGE) experiments under denaturing conditions with ODN sequences ^{32}P-radiolabeled at their 5′ extremities (Table 1) were performed to assess this photoreactivity. The results obtained after the blue-light irradiation of **1** in the presence of ODN_0 (ss and ds) and ODN_G (ss and ds) are shown in Figure 3.

When conjugate **1** is irradiated in the presence of (ss or ds) ODN_G (Figure 3, Lanes 2, 4, and 6 in the image on the right), a band with a lower electrophoretic mobility is observed, whereas no such bands can be detected with (ss or ds) ODN_0 (Figure 3, Lanes 2, 4, and 6 in the image on the left). These retarded bands with ODN_G are attributed to photo-crosslinking between **1** (through the Ru^{II} complex) and the G base of radiolabeled ODN_G (i.e., the formation of a photoadduct such as that in Figure 1, a). The irreversibly photo-crosslinked peptide–Ru–ODN_G product has not only a higher molecular weight but also additional positive charges that slow down the migration in the gel.

It should be noted that the ionic strength influences the photo-crosslinking yield, which is lower in conditions of higher ionic strength (see Figure 3, Lane 4 compared to 2 in the image on the right; Table 4). This difference is attributed to the weaker interaction between the ODN and **1** in presence of salt, which decreases the electrostatic interactions. The quantification of the different radiolabeled products also indicates that the yield

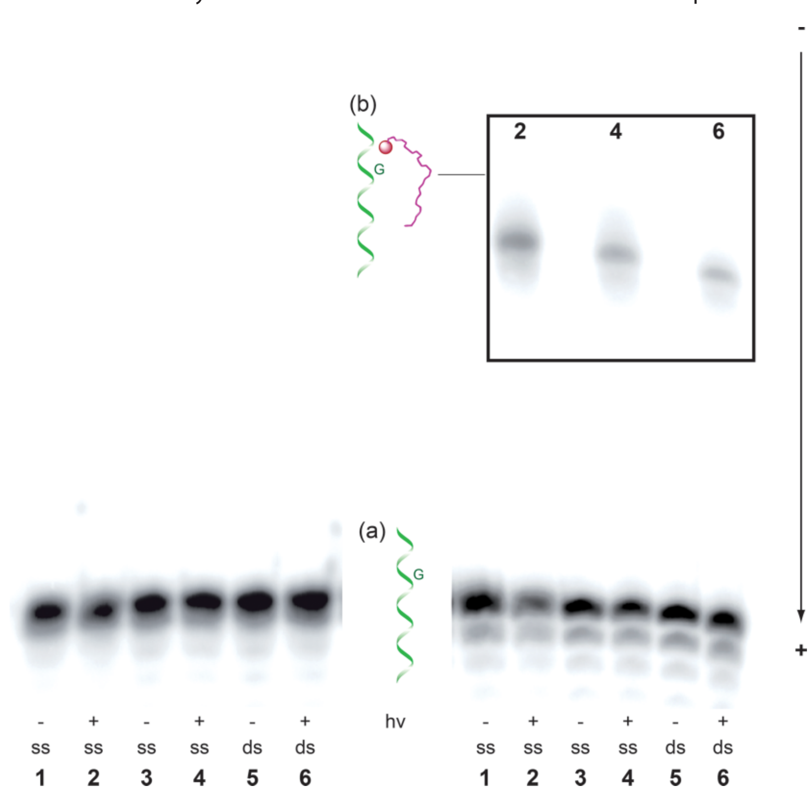

Figure 3. Polyacrylamide gel electrophoresis (PAGE 20 %) under denaturing conditions (urea 7 M) for samples containing **1** (5 µM) and ODN (5 µM) in aqueous solution (Tris/HCl 10 mM, pH 7), migration from top to bottom. Either radiolabeled ODN_0 (left) or ODN_G (right) was used. Lanes 1, 3, and 5 correspond to samples kept in the dark (–), and lanes 2, 4, and 6 correspond to samples irradiated for 20 min at λ = 405 nm (+). The ODNs are used as ss without salt (lanes 1–2) or in the presence of 50 mM NaCl as ss (lanes 3 and 4) or ds (lanes 5 and 6). The band declining from 1 to 6 on the right is an artefact of the experiment.

of photo-crosslinked **1**-ODN_G is slightly higher with $ssODN_G$ than with $dsODN_G$ (Table 4). This result seems surprising in regard to previous observations that the luminescence lifetime of the conjugate **1** with $dsODN_G$ is more strongly reduced than with $ssODN_G$. This apparent contradiction between these results can be explained easily. Indeed, the PET responsible for the shortening of the excited-state lifetime depends on the distance between the quencher (G base) and the Ru center, whereas the photoadduct (or photo-crosslinking) yield depends much more on the geometry adopted by the Ru–TAT conjugate (especially the position of the α-carbon atom to the TAP nitrogen atom) in front of the amino group of the G base.[35,36] The MD simulation provides an insight into these geometric constrains. Indeed, if the geometry is clearly more favorable for the $ssODN_G$ (Figure 2, b) owing to the relative freedom of the arrangement of the $ssODN_G$ strand, the situation is different for $dsODN_G$. In the structure obtained for the photo-crosslinked product (Figure 2, c), obtained by forcing the covalent bond between the TAP ligand and the amino group of G, there is a significant deformation of the duplex. The MD snapshot of the crosslinked structure **1**-$dsODN_G$ (Figure 2, c) shows that the G base has to flip out in this case to expose the guanine amino group to the exterior of the helix, as previously proposed.[35,36] This flip out of the G base as well as the partial duplex unfolding indicate a significant destabilization of the $dsODN_G$ in the photo-crosslinked structure that disfavors the formation of this photoadduct. Thus, even if the distance between the two atoms involved in the covalent bond to be formed is shorter for **1** with the $dsODN_G$ before the photoreaction, geometrical constraints lead to the observation of more favorable photo-crosslinking with $ssODN_G$. Thus, molecular modeling strengthens the PAGE results and shows that the formation of photo-crosslinked product **1**-$dsODN_G$ is less favored because of geometrical factors.

Table 4. PAGE experiments under denaturing conditions. Quantification of the retarded band attributed to the photoadduct between **1** and ODN.

Lane number as in Figure 3	Sequence[a]	C_{NaCl} [mM]	Photo-crosslinking[b] [%]
2 – left	$ssODN_0$	0	5
4 – left	$ssODN_0$	50	4
6 – left	$dsODN_0$	50	1
2 – right	$ssODN_G$	0	43
4 – right	$ssODN_G$	50	30
6 – right	$dsODN_G$	50	20

[a] The radiolabeled ODNs were irradiated for 10 min with a He/Cd laser (Melles Griot) at λ = 440 nm in the presence of **1** (5 µM), 10 mM Tris/HCl (pH 7), and either ssODN or dsODN. [b] The percentages of the photoproducts were determined as contributions relative to the sum of the intensity of all bands. Errors estimated to 5 %.

Cell Penetration

To assess the efficiency of the TAT peptide tethered to the Ru^{II} complexes for enhancing the cellular internalization of the resulting conjugate, we performed flow cytometry experiments with HeLa cells. HeLa cells were incubated in the presence of **1** or the photoluminescent conjugate **2** and, for comparison, in the presence of the corresponding nontethered $[Ru(phen)_3]^{2+}$ complex at various concentrations. The HeLa cells were protected from direct light during the incubation process to avoid photoinduced cell internalization.[11] As expected, we were unable to detect luminescence from cells incubated with **1** (1 µM). This absence of luminescence could be anticipated a priori, as conjugate **1** is photoreactive and, thus, its luminescence could be quenched inside the cells (see below). Although the free $[Ru(phen)_3]^{2+}$ complex cannot cross the cell membrane, a dramatic increase of internalization of this complex by the cells was induced by tethering the complex to the TAT peptide. Indeed, at a concentration of 1 µM, at which free $[Ru(phen)_3]^{2+}$ barely penetrates inside HeLa cells with a transfection yield of 0.2 %, conjugate **2** shows 27 % transfection (Figure SI3). At a higher concentration of **2** (10 µM), a transfection yield of 65 % was reached. Thus, the concept of anchoring TAT peptide onto $[Ru(phen)_3]^{2+}$ was demonstrated, as it allows the incorporation of the complex. The photoreactivity of the Ru–TAP complex prevented the use of flow cytometry to confirm the cellular internalization of **1**. As $[Ru(phen)_3]^{2+}$ and $[Ru(TAP)_3]^{2+}$ share a similar geometry, we could postulate that conjugate **1** should a priori behave similarly to photoluminescent conjugate **2** regarding the TAT properties that allow the cellular penetration. However, another technique that does not rely on the luminescence of the Ru^{II} complex was used to assay the cellular penetration.

ICP-MS measurements were performed with HeLa cells to quantify the cellular uptake of both **1** and **2**. The influence of the transfection time was investigated for conjugate **2**. HeLa cells were treated with 2.5 µM of conjugate **2** for 30, 60, 120, and 200 min. After thorough washing, the cells were lysed, and the whole-cell lysates were analyzed for their ruthenium content by ICP-MS for each sample and normalized to the protein content. As shown in Figure 4, after a transfection time of 30 or 60 min, the intracellular concentration conjugate **2** was (21 ± 1) $ng_{Ru}/mg_{protein}$. This intracellular concentration remains constant over 1 h.

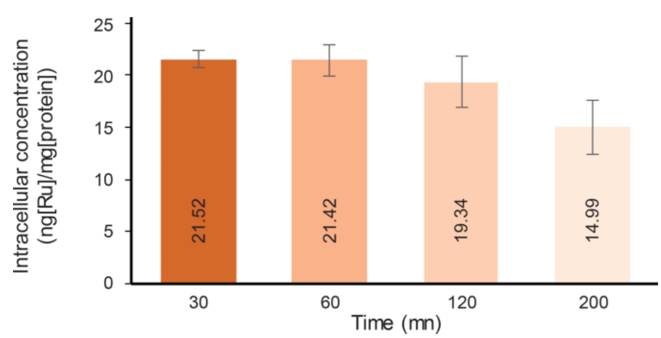

Figure 4. ICP-MS assay for the whole-cell ruthenium accumulation. HeLa cells were treated with 2.5 µm of Ru–TAT conjugate **2** for 30, 60, 120, and 200 min. The cells were analyzed for their ruthenium content by ICP-MS. The ruthenium amount was normalized to the protein content, which was determined by Bradford assay.

On the basis of these results, a transfection time of 30 min was chosen for the following experiments. HeLa cells were treated with different concentrations of **1** and **2** for 30 min, and the whole-cell lysate was analyzed to determine the ruthenium levels by ICP-MS and normalized to the protein content (Figure 5). For comparison, the experiments were also performed with $[Ru(phen)_3]^{2+}$ and $[Ru(DIP)_2phen]^{2+}$ (see Supporting Information).

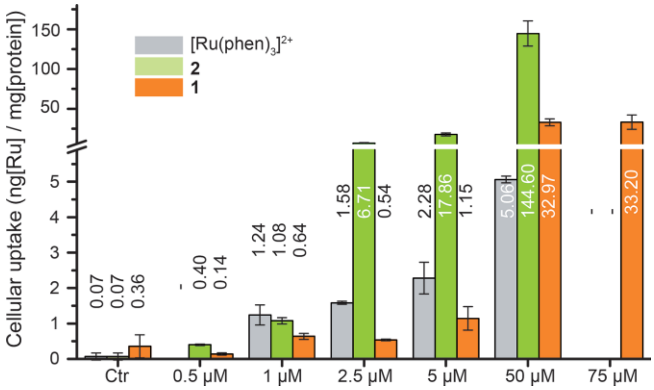

Figure 5. ICP-MS assay for the whole-cell ruthenium accumulation. HeLa cells were treated with different concentrations of free $[Ru(phen)_3]^{2+}$ and the Ru–TAT conjugates **1** and **2** for 30 min. The cells were analyzed for the ruthenium contents by ICP-MS. The ruthenium amounts were normalized to the protein content, which was determined by Bradford assay. Ctr corresponds to the negative control in which the cells were not treated with any Ru complex or conjugate.

As expected and consistent with the results obtained by flow cytometry (see above), free $[Ru(phen)_3]^{2+}$ exhibits a penetration rate close to zero at 1 µM. $[Ru(DIP)_2phen]^{2+}$ bearing two DIP ligands, which improve cellular uptake dramatically,[9] shows penetration rates of (1.68 ± 0.10) and (4.46 ± 0.24) $ng_{Ru}/mg_{protein}$ at 1 and at 5 µM, respectively (Figure SI4). Thus, the internalization of $[Ru(DIP)_2phen]^{2+}$ was confirmed. However, in comparison, the uptake for conjugate **2** at 5 µM is much higher [(17.86 ± 1.77) $ng_{Ru}/mg_{protein}$]. Conjugate **2** reveals an increased internalization as a function of the external applied concentration: it rises from (1.08 ± 0.09) $ng_{Ru}/mg_{protein}$ at 1 µM to (144.60 ± 15.73) $ng_{Ru}/mg_{protein}$ at 50 µM. In contrast, conjugate **1** exhibits a slightly lower cellular uptake as a function of the external applied concentration; the intracellular concentration at 1 µM is very low [(0.64 ± 0.08) $ng_{Ru}/mg_{protein}$] and it increases slightly to (32.97 ± 4.45) $ng_{Ru}/mg_{protein}$ at 50 µM concentration, at which a plateau seems to have been reached. Indeed, at 75 µM, the intracellular concentration is more or less the same. In contrast to our initial hypothesis, the two Ru–TAT conjugates exhibit different cellular internalization behavior, and conjugate **2** exhibits a greater uptake than that of conjugate **1**.[37] However, both **1** and **2** show a large improvement of cell penetration in comparison with those of the unmodified complexes $[Ru(phen)_3]^{2+}$ and $[Ru(TAP)_2phen]^{2+}$; thus, these results confirm the role of the TAT peptide.

Photocytotoxicity against HeLa Cells

The internalization of **1** should induce a significant photocytotoxicity owing to its photoreaction through a PET process with the guanine bases of DNA or RNA. Conjugate **2** could also be photoactive but through an oxygen photosensitization process. Thus, the cytotoxicities and photocytotoxicities of **1**, **2**, and the free reference complexes {$[Ru(phen)_3]^{2+}$ and $[Ru(TAP)_2(phen)]^{2+}$} were evaluated by MTT assays. For the free complexes tested in the dark or after blue-light irradiation, negligible cytotoxicities and photocytotoxicities were observed (Figure SI5). Indeed, only 5–10 % of mortality was obtained independently of the concentration of the complexes. This confirms that both complexes are unable to penetrate into the cells (in the dark), and the illumination does not affect the cell viability in this case.

Concerning conjugates **1** and **2**, as the ICP-MS results showed that they have different penetration rates (Figure 5), we performed MTT assays with these two conjugates at the same intracellular concentration with different external incubation concentrations but the same incubation time (higher external concentration for **1** than for **2**, see Table 5). The survival rates of the HeLa cells under such conditions (i.e., for the same intracellular concentrations) are shown in Table 5. At 1 $ng_{Ru}/mg_{protein}$ intracellular concentration, there is almost no toxicity for both **1** and **2** either in the dark or under irradiation. With a higher intracellular concentration of 25 $ng_{Ru}/mg_{protein}$, an effect on the survival rate was observed for conjugate **2**. Indeed, the survival rate dropped by 50 % under irradiation. However, more surprisingly, no effect was observed for the irradiation of cells treated with **1**, and their survival yield was unaffected.

This observation was quite unexpected. Indeed, it means that even at the same intracellular concentration, conjugate **2** has a far greater photocytotoxic effect on HeLa cells than conjugate **1**, despite the capacity of conjugate **1** to photoreact with DNA and RNA in vitro and to form photoadducts. A possible explanation would be that conjugate **1** has no access to the genetic material so that no photoelectron transfer could take place and the DNA photoadduct could not form.

To confirm this hypothesis, confocal microscopy was performed on HeLa cells incubated with conjugates **1** and **2**. A specific marker of nuclei (Draq5) was used to stain the cell nuclei to obtain information on the localization of the tethered complexes inside the cells. The pictures are shown in Figure 6. To enable the observation of both conjugates **1** and **2** inside the cells, we used a concentration of 50 µM of **1** and **2** for the confocal microscopy experiments. A negative control (Figure SI6) experiment was also performed to detect possible autofluorescence of the HeLa cells. In Figure 6 (b), the intracellular

Table 5. Survival rate of HeLa cells determined by MTT assays for the same intracellular concentrations, as determined by ICP-MS measurements.

	Conjugate **2**		Conjugate **1**	
Applied concentration [µM]	1	9	5	35
Intracellular concentration [$ng_{Ru}/mg_{protein}$]	1	25	1	25
Survival in the dark [%][a]	85 ± 10	76 ± 10	103 ± 9	106 ± 12
Survival under light [%][a]	100 ± 16	51 ± 10	109 ± 13	113 ± 15

[a] Cells were incubated with Ru–TAT conjugate for 2 h and then washed and irradiated for 2 h. The MTT assay was performed after 24 h. The survival rate [%] was calculated relative to untreated and nonirradiated cells. The measurements were performed twelve times.

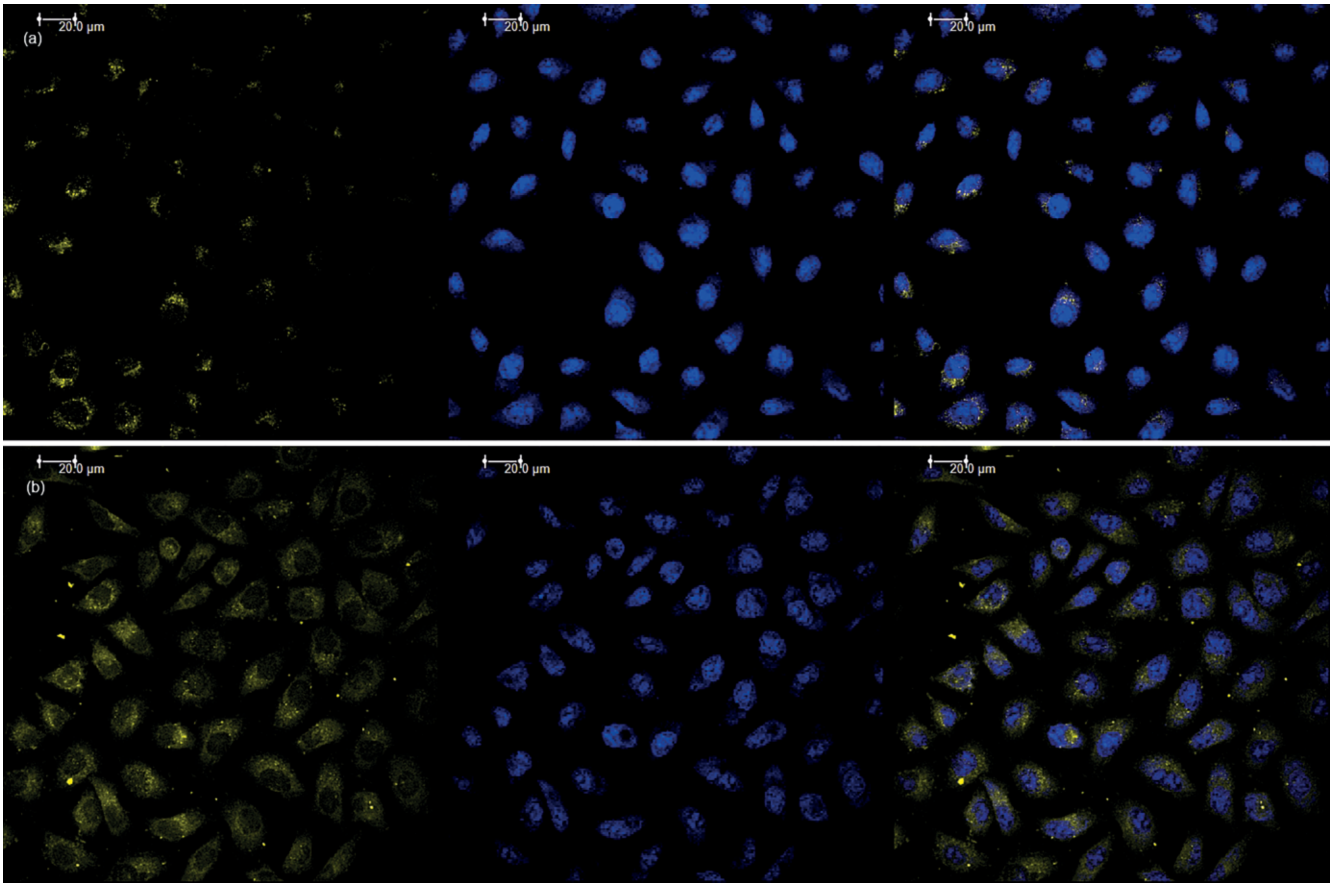

Figure 6. Confocal imaging of HeLa cells incubated with 50 µM of (a) **1** and (b) **2** for 30 min. The luminescence of the Ru^{II} complex is yellow (left),[38] and the cell nuclei were labeled with Draq5 (blue: middle). The absence of colocalization in the overlay (right) indicates that the ruthenium conjugates are not internalized in the cell nuclei but are localized inside the cytoplasm.

distribution of conjugate **2** can be observed as a diffuse staining in the cytoplasm with localization within endosomal and endoplasmic reticulum vesicles. The intracellular distribution of conjugate **1** (Figure 6, a) is very similar to that observed for **2**. Thus, confocal microscopy indicates that both conjugates **1** and **2** are mainly localized in the vesicles and in the cytoplasm but not inside the nuclei.

This localization of both conjugates could be at the origin of the absence of photocytotoxicity for **1**, which has no access to the genetic material. This would also be the case for conjugate **2**. However, **2** would probably be able to produce much more $^1O_2^*$ than **1** by photosensitization. As singlet oxygen can probably induce rupture of the endosomal membranes, **2** would be liberated and free to generate cellular damage and, thus, induce photocytotoxicity, as observed experimentally.

To support this hypothesis, the yields of singlet-oxygen photosensitization by the two free complexes $[Ru(TAP)_2(phen)]^{2+}$ and $[Ru(phen)_3]^{2+}$ were compared. As shown in Table 6, the quantum yield of $^1O_2^*$ production for $[Ru(phen)_3]^{2+}$ is twice that for $[Ru(TAP)_2(phen)]^{2+}$ in H_2O (0.22 vs. 0.13). Thus, the TAP complex is not as good a photosensitizer as the phen complex. It should also be noted that excited $[Ru(TAP)_2(phen)]^{2+}$ could be quenched inside the cytoplasm by other quenchers such as tryptophan and tyrosine[39–42] through a PET process. In addition to a lower singlet-oxygen photosensitization yield and an endosomal localization, this quenching would likely make conjugate **1** inefficient for the induction of cell death through the formation of DNA photoadducts.

Table 6. Quantum yield of singlet-oxygen production from photosensitization by $[Ru(TAP)_2phen]^{2+}$ and $[Ru(phen)_3]^{2+}$ in water.

Complex	τ_{air} [ns] [a]	τ_{argon} [ns] [a]	$\Phi_{\Delta}air$[b]
$[Ru(phen)_3]^{2+}$	505	933	0.22
$[Ru(TAP)_2phen]^{2+}$	724	840	0.13

[a] Errors estimated to 5 %. [b] The quantum yield of singlet-oxygen photosensitization in water under air was calculated from the experimental data with oxygen-saturated D_2O solutions (see Experimental Section).

Conclusions

This study shows that the tethering of Ru–TAP complexes to the TAT peptide does not induce a decrease of the photoreactivity towards oligonucleotides containing at least one G base. The ICP-MS technique leads to the conclusion that the TAT peptide helps Ru–TAP complexes to penetrate inside the cells but at a lower concentration than that of the reference complex $[Ru(phen)_3]^{2+}$. This shows that the properties of the cargo of the Ru complex can also influence the TAT penetration. Nevertheless, for the same Ru concentration inside the cell, conjugate

1 does not induce cellular death, whereas conjugate **2** does. The difference likely originates from their different mechanisms of action under irradiation. Indeed, Ru–TAP complexes are very efficient for inducing a PET with the guanine bases of DNA, as shown in several previous studies.[4,28,29] The present results show that the TAT peptide transports the Ru complex mainly into vesicles and into the cytoplasm; therefore, the Ru–TAP complex cannot reach its DNA or RNA targets. In contrast, the Ru–phen complex also transported into the vesicles by the TAT peptide can behave as an excellent singlet-oxygen photosensitizer, which is not the case for the Ru–TAP complex. Thanks to this singlet-oxygen generation, the Ru–phen complex could be liberated from endosomes into the cytoplasm to find different targets, which explains the cell death.

This work emphasizes that photoactivable drugs such as Ru–TAP complexes can become quite inefficient if their transporters such as the TAT peptide deliver their cargo to cellular sites isolated from the targets, even if the drugs are very efficient for damaging genetic material.[28,29]

Experimental Section

Synthesis: Conjugates **1** and **2** (Figure 1, b) were synthesized as described previously.[32,33] Briefly, a modified phenanthroline ligand bearing an aminooxy group was coordinated to the desired bischelated precursor {either $[Ru(TAP)_2Cl_2]$ or $[Ru(phen)_2Cl_2]$}. TAT peptide [corresponding to the 48–57 residues of the trans-activating transcriptional (tat) protein of HIV-1] containing an extra N-terminal serine group (**3**) was oxidized to yield N-terminal aldehyde-containing peptide (**4**), which was subsequently reacted with the aminooxy function of the complex to form the final oxime ligation product. The so-obtained Ru^{II}–TAT conjugates **1** and **2** were purified by preparative HPLC and characterized by HRMS (Figures S1 and SI7).

Thermal Denaturation Experiments: Before the thermal denaturation experiments of ODN_0 and ODN_G (the sequences are presented in Table 1), the ODN duplexes [2 µM in tris(hydroxymethyl)aminomethane/HCl (Tris/HCl) buffer 10 mM, pH 7, and 50 or 150 mM NaCl] were annealed at 90 °C for 10 min and then cooled to room temperature. The absorbance at λ = 260 nm was monitored as a function of temperature between 10 and 60°. Three cycles were performed at a rate of 1 °C/min with a Perkin–Elmer Lambda 35 UV/Vis spectrophotometer with a 0.1 °C step, controlled by a PTP-1 Peltier temperature programmer and a temperature-sensor accessory. The absorbance was recorded with the program TEMPLAB 2.00. The melting temperatures were determined by fitting the data in the MATLAB 7.1 software.

Lifetime Measurements: The luminescence lifetimes were measured by TC-SPC with an Edinburgh Instruments FL900 spectrometer equipped with a hypobaric nitrogen-filled discharge lamp pulsed at 30 kHz and a red-sensitive, Peltier-cooled photomultiplier (R928, Hamamatsu). The samples were kept at (20 ± 2) °C with a Haake NB22 temperature controller. The sample was excited at λ = 379 nm, and the emission was measured at the maximum emission of the complex (λ = 640 nm). The data were collected by a multichannel analyzer (2048 channels) with the minimum number of counts in the first channel (t = 0) equal to 10^4. The resulting decays were analyzed with the Edinburgh Instruments software (version 3.0), deconvoluted for the instrumental response, and fitted to exponential functions based on nonlinear least-squares regressions using a modified Marquardt algorithm. The reduced χ^2, weighted residuals, and autocorrelation function were employed to judge the quality of the fits.

Singlet-Oxygen Photosensitization: The quantum yield of singlet-oxygen production was measured through the time-resolved detection of the $^1O_2$ phosphorescence at λ = 1270 nm. Solutions of the complexes (sample and reference, both as chloride salts) were prepared in D_2O with a matched absorbance of 0.40 at λ = 532 nm. The solutions were purged thoroughly with O_2 or argon for a minimum of 30 min. The experiments were performed with an Edinburgh Instruments (UK) LP-900 laser kinetic spectrometer system equipped with a Nd:YAG laser (Minilite II, Continuum, CA) for excitation at λ = 532 nm and a Hamamatsu H10330-45 NIR photomultiplier tube (PMT) for singlet-oxygen emission monitored at λ = 1260 nm (Bentham TM300 monochromator) with a 10 kΩ resistance at the signal output for proper amplification. An Ophir AN/2 energy meter with a thermopile head (Ophir Optronics Ltd., Israel) was employed to monitor the energy of the laser pulse (E), which was varied from 100 to 500 µJ/pulse to avoid even partial saturation of the emission signal and keep it in the linear region. The near-IR (NIR) emission from the sample was monitored at 90° with respect to the excitation pathway and detected with the NIR PMT after passing through an interference filter centered at λ = 1265 nm [77 nm full width at half-maximum (FWMH), Roithner Laser]. Typically, 40 laser shots were averaged for each signal to improve the signal-to-noise (s/n) ratio. All of the $^1O_2$ luminescence decay profiles were fitted to an exponential function after the exclusion of the fast decay of the Ru^{II} sensitizer emission even under O_2 saturation. The $^1O_2$ luminescence lifetime was checked frequently (at least at the beginning and end of the series of the measurements at different laser energies); in every case, it was coincident with the literature value [(62 ± 4) µs in D_2O].

After the extrapolation of the intensities of the $^1O_2$ signal at zero time with the exponential decay curve and the calculation of the area under the curve (S) for the sample and reference at the different laser energies (Origin 9.0), the respective regression lines were built. The Φ_Δ value of the unknown solution was calculated from the following equation with $[Ru(phen)_3]^{2+}$ as the reference (Φ_Δ^{ref} = 0.39 ± 0.03 in 100 % O_2-saturated D_2O at room temperature): [43]

$$\Phi_\Delta^{sample} = \Phi_\Delta^{ref}\left(\frac{slope_{sample}}{slope_{ref}}\right)$$

The quantum yields of singlet-oxygen production in oxygen-saturated solutions of the complexes in D_2O are presented in Table SI8.

The quantum yields of singlet-oxygen production under other conditions (H_2O/air) were further estimated from the luminescence lifetimes of the complexes under these conditions, with the assumption that the fraction of quenched triplets by oxygen to yield $^1O_2$ ($f_\Delta{}^T$) is the same in D_2O and H_2O, by using the following equations:

$$\Phi_\Delta = \Phi_T P_{O_2}^T f_\Delta^T$$

$$P_{O_2}^T = \tau k_q[\mathbf{O_2}] = 1 - \frac{\tau}{\tau_0}$$

Φ_T is the quantum yield of formation of the excited triplet metal-to-ligand charge-transfer (^{3}MLCT) state (considered as 1), $P_{O_2}^T$ is the proportion of triplet excited states quenched by O_2, and $f_\Delta{}^T$ is the yield of $^1O_2$ produced by the quenching. $P_{O_2}^T$ can be expressed as a function of the ratio of the excited-state lifetimes of the complex in the absence and presence of oxygen. From the luminescence lifetimes of the complex under different conditions, the quantum yield of singlet-oxygen photosensitization in water under air can be calculated through the relationship:

$$\Phi^{Air}_{\Delta H_2O} = \Phi^{O_2}_{\Delta D_2O}\left(1-\tau^{H_2O}_{Air}/\tau^{H_2O}_{Ar}\right)\Big/\left(1-\tau^{D_2O}_{O_2}/\tau^{D_2O}_{Ar}\right)$$

PAGE Experiments: For the gel electrophoresis experiments, ODNs were 5′-end-labeled by T4 polynucleotide kinase (Roche Belgium) with γ-[^{32}P]-ATP (3000 Ci/mmol, Perkin–Elmer Life Sciences) at 37 °C for 20 min. The ODN duplex solutions were prepared by mixing equimolar solutions of each ODN and complementary strands. The ODNs were hybridized at 90 °C for 10 min and then cooled to room temperature overnight. The samples were prepared with 3 µM ODN (ssODN or dsODN), 3 µM of **1**, 0 or 50 mM of NaCl, and 10 mM of Tris/HCl buffer (pH 7). The samples were illuminated for 10 min with a 442 nm He/Cd laser (Melles Griot He/Cd Laser Omnichrome LC-500). The sample (10 µL) was added to the loading buffer (95 % formamide, 0.1 % xylene cyanol, and 0.1 % bromophenol blue). The mixture was loaded on polyacrylamide gel (20 % with a 19:1 acrylamide/bisacrylamide ratio) containing 7 M urea in a TBE buffer [90 mM Tris-borate and 2 mM ethylenediaminetetraacetic acid (EDTA)]. After migration, the gel was exposed to a Phosphor Imager screen overnight at 3 °C. The screen was scanned with a Phosphor Imager Storm 860 (Amersham Pharmacia Biotech) instrument.

Molecular Modeling: The initial structure of the Ru–TAT conjugate was obtained by linking the Ru^{II} complex (structure obtained by DFT calculations)[44] to the linker + TAT peptide in α-helical conformation, as suggested previously.[45] The Ru^{II} complex was constrained in an octahedral geometry with harmonic restraints for subsequent MD simulations. From selected structures from the preliminary MD simulations for noncovalent Ru–TAT/ODN complexes, the structures of the Ru–TAT–ODN covalent adducts were obtained as described previously.[46] The MD simulations of Ru–TAT and Ru–TAT–ODN were performed with the CHARMM force-field,[47] and water was considered explicitly through the use of the water box model. The MD simulations were performed in (*N,V,T*) at 300 K with a time step of 1 fs from 1 ns to 10 ns. The calculations, analysis, and visualization were performed with DS 4.0 package from Biovia and the Chimera program.[48]

Flow Cytometry: HeLa cells were grown over 2 d at 37 °C in a humidified atmosphere with 5 % CO_2 in Dulbecco's modified Eagle medium (DMEM, without phenol red) in six-well plates to reach a density of ca. 800000 cells/well. The cells were washed twice with phosphate-buffered saline (PBS). OptiMEM medium containing the desired concentration of an aqueous solution of the complexes (never exceeding 1 % v/v) was added. The cells were incubated in the dark at 37 °C for 30 min. To remove noninternalized complexes, the cells were washed three times with OptiMEM medium and then trypsinized and resuspended in PBS for the analysis of their emission. The flow cytometric data were acquired with a FACS Calibur flow cytometer (BD Biosciences) and analyzed by the Cellquest software (BD Biosciences). The mean luminescence values were calculated with the Cellquest software. An argon laser (λ = 405 nm) was used for the excitation of the complexes, and the emission was detected at λ > 502 nm. Side- and forward-scattered light from a second laser at λ = 488 nm was used to exclude debris.

ICP-MS Experiments for Ruthenium Content of the Whole Cell: HeLa cells were plated at 400000 cells/well in a six-well plate. The cells were allowed to adhere for 24 h and then treated with 700 µM of different concentrations of the complexes. After 30 min of incubation in the dark, the media were eliminated, and the cell monolayer was washed three times with PBS (1 mL). PBS (800 µL) was added to the cells, which were then scratched from the plate. The resuspended cells were then lysed by sonication with a Bioruptor processor (Diagenode) for 15 min at the highest amplitude in ice. The lysate (750 µL) was then combined with a 2 % HNO_3 (v/v) solution (750 µL). The remaining lysate was quantified for protein by Bradford assay; the absorption of the dye (Coomassie blue) used for this assay was measured at λ = 595 nm, at which the absorption of the Ru complexes is negligible. It was not expected that the Ru complex or the TAT peptide would interfere with the determination of the protein concentrations. The ruthenium content of the solution was analyzed with an Agilent 7700x quadrupole ICP-MS unit with a He collision cell. The ruthenium levels were normalized as a function of the protein amount determined by the Bradford assay and expressed as $ng_{Ru}/mg_{protein}$. For each set of conditions (concentration of the complex, incubation time of the complex), three independent experiments were performed, and the errors were calculated from those three independent measurements.

Photocytotoxicity Experiments: HeLa cells were cultured in a 96-well plate for 1 d in DMEM (without phenol red) to reach 80 % confluence. The cells were rinsed, and fresh medium containing the desired concentration of the complexes was added. After 2 h of incubation at 37 °C in the dark, the cells were rinsed twice to remove noninternalized complexes. Illumination was performed with five 20 W white bulbs, and a 0.1 M $NaNO_2$ solution was used to filter UV light. The distance between the light source and the culture plate was 25 cm. Before illumination, the cultures were rinsed with PBS and illuminated in PBS to avoid absorption by colored culture medium. Plates serving as a dark control were placed on the illumination block but protected from illumination with aluminum foil. All of the cultures were kept on a heating block set at 37 °C during the 2 h of illumination. Illuminated and control cultures were returned immediately to the incubator at 37 °C in a humidified environment and cultured in culture medium for an additional 24 h. The cell viability was measured 1 d postirradiation through MTT assay (Vybrant® MTT Cell Proliferation Assay Kit, Life-Technologies). The cells were incubated for 3 h with the MTT solution, and then SDS•HCl (SDS = sodium dodecyl sulfate) solution was added to each well to solubilize the precipitated formazan as described in the Vybrant® MTT Cell Proliferation Assay Kit protocol. The cells were incubated for 3 h, and then the developed color of the formazan derivative was read with a spectrophotometer at λ = 570 nm. The ratio of the optical density (OD) at λ = 570 nm under each set of conditions relative to that of the control cells (nontransfected and nonirradiated, 100 % viability) was used to determine a relative viability. The measurements were performed twelve times.

Confocal Laser Scanning Microscopy: HeLa cells were grown at 37 °C in a humidified atmosphere with 5 % CO_2 in DMEM medium without phenol red, seeded on round coverslips at a density of ca. 80000 cells/coverslip, and cultured for 2 d. The cells were transfected with 50 µM autoluminescent **1** and **2** for 2 h in the dark. After this incubation, the medium containing the complex was removed, and fresh medium was added to the cells. The cells were rinsed in prewarmed PBS, fixed in 4 % paraformaldehyde for 10 min, labeled with Draq5 following instructions of the manufacturer, and finally mounted in Mowiol. A confocal laser scanning microscopy system (Leica TCS SP5 RS) was used to acquire confocal luminescence images. An argon laser (λ = 405 nm) was used for the excitation of the Ru^{II} complexes, and a helium–neon laser (λ = 633 nm) was used for the excitation of the nuclear dye Draq5 (1,5-bis{[2-(methylamino)ethyl]amino}-4,8-dihydroxyanthracene-9,10-dione, eBiosciences).

Acknowledgments

The authors gratefully thank N. Matielli and J. De Jong (G-Time Lab at the U. L. B.) for the ICP-MS measurements. We also acknowledge gratefully Professor Guillermo Orellana for the measurements of singlet-oxygen quantum yields realized at the Universidad Complutense de Madrid. This research was supported by the Interuniversity Attraction Poles Programme (P7/05 and P07/32) of the Belgian Science Policy Office and by the "Fonds National pour la Recherche Scientifique" (FNRS) under grant numbers 2.4615.11 and 2.4530.12. The Nanobio-ICMG platform (FR 2607) in Grenoble is acknowledged for providing facilities for the synthesis and purification of conjugates. L. M. and J. G. are grateful to the Fonds de la Recherche Scientifique – FNRS (F.R.S.-FNRS) for a PhD grant. S. K. thanks the Fonds pour la Formation à la Recherche dans l'Industrie et dans l'Agriculture (F.R.I.A.) for a PhD grant. M. S. is Research Associate of the F.R.S.-FNRS. G. F. was supported by a grant from the Télévie (F.R.S.-FNRS).

Keywords: Bioinorganic chemistry · Medicinal chemistry · Photochemistry · Ruthenium · N ligands · Peptides

[1] A. E. Friedman, J. C. Chambron, J. P. Sauvage, N. J. Turro, J. K. Barton, *J. Am. Chem. Soc.* **1990**, *112*, 4960–4962.
[2] C. Moucheron, A. Kirsch-De Mesmaeker, S. Choua, *Inorg. Chem.* **1997**, *36*, 584–592.
[3] H. Song, J. T. Kaiser, J. K. Barton, *Nat. Chem.* **2012**, *4*, 615–620.
[4] L. Marcélis, J. Ghesquière, K. Garnir, A. Kirsch-De Mesmaeker, C. Moucheron, *Coord. Chem. Rev.* **2012**, *256*, 1569–1582.
[5] L. Marcélis, C. Moucheron, A. Kirsch-De Mesmaeker, *Philos. Trans. R. Soc. A* **2013**, *371*.
[6] M. Demeunynck, C. Moucheron, A. Kirsch-De Mesmaeker, *Tetrahedron Lett.* **2002**, *43*, 261–264.
[7] L. Marcélis, W. Vanderlinden, A. Kirsch-De Mesmaeker, *Probing DNA Using Metal Complexes*, in: *Inorganic Chemical Biology: Principles, Techniques and Applications* (Ed.: G. Gasser), John Wiley & Sons, Chichester, UK, **2014**.
[8] L. Jacquet, J. M. Kelly, A. Kirsch-De Mesmaeker, *J. Chem. Soc., Chem. Commun.* **1995**, 913–914.
[9] C. A. Puckett, J. K. Barton, *J. Am. Chem. Soc.* **2007**, *129*, 46–47.
[10] M. R. Gill, J. Garcia-Lara, S. J. Foster, C. Smythe, G. Battaglia, J. A. Thomas, *Nat. Chem.* **2009**, *1*, 662–667.
[11] J. W. Dobrucki, *J. Photochem. Photobiol. B* **2001**, *65*, 136–144.
[12] M. E. Jimenez-Hernandez, G. Orellana, F. Montero, M. T. Portoles, *Photochem. Photobiol.* **2000**, *72*, 28–34.
[13] C. A. Puckett, J. K. Barton, *Biochemistry* **2008**, *47*, 11711–11716.
[14] F. R. Svensson, M. Matson, M. Li, P. Lincoln, *Biophys. Chem.* **2010**, *149*, 102–106.
[15] F. R. Svensson, M. Li, B. Nordén, P. Lincoln, *J. Phys. Chem. B* **2008**, *112*, 10969–10975.
[16] D. Garcìa-Fresnadillo, Y. Georgiadou, G. Orellana, A. M. Braun, E. Oliveros, *Helv. Chim. Acta* **1996**, *79*, 1222–1238.
[17] H. Huang, B. Yu, P. Zhang, J. Huang, Y. Chen, G. Gasser, L. Ji, H. Chao, *Angew. Chem. Int. Ed.* **2015**, *54*, 14049–14052; *Angew. Chem.* **2015**, *127*, 14255.
[18] F. Svensson, J. Andersson, H. Åmand, P. Lincoln, *J. Biol. Inorg. Chem.* **2012**, *17*, 565–571.
[19] R. B. P. Elmes, K. N. Orange, S. M. Cloonan, D. C. Williams, T. Gunnlaugsson, *J. Am. Chem. Soc.* **2011**, *133*, 15862–15865.
[20] K. K. W. Lo, T. K. M. Lee, J. S. Y. Lau, W. L. Poon, S. H. Cheng, *Inorg. Chem.* **2008**, *47*, 200–208.
[21] C. A. Puckett, J. K. Barton, *Bioorg. Med. Chem.* **2010**, *18*, 3564–3569.
[22] A. Martin, A. Byrne, C. S. Burke, R. J. Forster, T. E. Keyes, *J. Am. Chem. Soc.* **2014**, *136*, 15300–15309.
[23] L. Cosgrave, M. Devocelle, R. J. Forster, T. E. Keyes, *Chem. Commun.* **2010**, *46*, 103–105.
[24] J. D. Ramsey, N. H. Flynn, *Pharmacol. Ther.* **2015**, *154*, 78–86.
[25] T. Skotland, T. G. Iversen, M. L. Torgersen, K. Sandvig, *Molecules* **2015**, *20*, 13313–13323.
[26] M. Zahid, P. D. Robbins, *Molecules* **2015**, *20*, 13055–13070.
[27] U. Neugebauer, Y. Pellegrin, M. Devocelle, R. J. Forster, W. Signac, N. Moran, T. E. Keyes, *Chem. Commun.* **2008**, 5307–5309.
[28] A. Reschner, S. Bontems, S. Le Gac, J. Lambermont, L. Marcélis, E. Defrancq, P. Hubert, C. Moucheron, A. Kirsch-De Mesmaeker, M. Raes, J. Piette, P. Delvenne, *Gene Ther.* **2013**, *20*, 435–443.
[29] L. Marcélis, N. Van Overstraeten-Schlögel, J. Lambermont, S. Bontems, N. Spinelli, E. Defrancq, C. Moucheron, A. Kirsch-De Mesmaeker, M. Raes, *ChemPlusChem* **2014**, *79*, 1597–1604.
[30] O. Lentzen, E. Defrancq, J. F. Constant, S. Schumm, D. Garcia-Fresnadillo, C. Moucheron, P. Dumy, A. Kirsch-De Mesmaeker, *J. Biol. Inorg. Chem.* **2004**, *9*, 100–108.
[31] H. Brooks, B. Lebleu, E. Vivès, *Adv. Drug Delivery Rev.* **2005**, *57*, 559–577.
[32] S. Deroo, E. Defrancq, C. Moucheron, A. Kirsch-De Mesmaeker, P. Dumy, *Tetrahedron Lett.* **2003**, *44*, 8379–8382.
[33] M. Villien, S. Deroo, E. Gicquel, E. Defrancq, C. Moucheron, A. Kirsch-De Mesmaeker, P. Dumy, *Tetrahedron* **2007**, *63*, 11299–11306.
[34] The impossibility of distinguishing a third very short component for $ssODN_G$ is attributed to the greater flexibility of **1**–$ssODN_G$, which prevents a clear distinction between different environments of the excited complex.
[35] S. Le Gac, M. Surin, E. Defrancq, C. Moucheron, A. Kirsch-De Mesmaeker, *Eur. J. Inorg. Chem.* **2013**, 208–216.
[36] L. Marcélis, M. Surin, R. Lartia, C. Moucheron, E. Defrancq, A. Kirsch-De Mesmaeker, *Eur. J. Inorg. Chem.* **2014**, 3016–3022.
[37] Conjugate **2** exhibits a linear increase in uptake with increasing concentrations applied to the HeLa cells, whereas conjugate **1** reveals not only a reduced uptake at the same concentration in comparison to that of **2** but also a nonlinear dependence upon the applied concentration, as a plateau is observed with a maximal value at ca. 33 $ng_{Ru}/mg_{protein}$ internalized. A theoretical approach showed that $[Ru(TAP)_2phen]^{2+}$ is more hydrophilic than its analogue $[Ru(phen)_3]^{2+}$, and this can explain these differences.
[38] It should be noted that the luminescence from **1** is clearly weaker than that observed for **2**. This difference can be explained by two factors: (1) the internalization of **1** is lower than that for **2**, (2) the luminescence of **1** can be quenched by a PET process between $[Ru(TAP)_2phen]^{2+}$ and the amino acid residues such as tryptophan and tyrosine[39–42] of the proteins encountered by the conjugate within the cell.
[39] N. Gauthier, J. De Winter, P. Gerbaux, C. Moucheron, M. Luhmer, A. Kirsch-De Mesmaeker, *Inorg. Chem.* **2010**, *49*, 6796–6798.
[40] J. Ghesquière, N. Gauthier, J. De Winter, P. Gerbaux, C. Moucheron, E. Defrancq, A. Kirsch-De Mesmaeker, *Chem. Eur. J.* **2012**, *18*, 355–364.
[41] M. Rebarz, J. Ghesquière, A. Boisdenghien, E. Defrancq, C. Moucheron, A. Kirsch-De Mesmaeker, *Inorg. Chem.* **2010**, *49*, 10867–10874.
[42] E. Gicquel, A. Boisdenghien, E. Defrancq, C. Moucheron, A. Kirsch-De Mesmaeker, *Chem. Commun.* **2004**, 2764–2765.
[43] A. Hergueta-Bravo, M. E. Jiménez-Hernandez, F. Montero, E. Oliveros, G. Orellana, *J. Phys. Chem. B* **2002**, *106*, 4010–4017.
[44] L. Ghizdavu, F. Pierard, S. Rickling, S. Aury, M. Surin, D. Beljonne, R. Lazzaroni, P. Murat, E. Defrancq, C. Moucheron, A. Kirsch-De Mesmaeker, *Inorg. Chem.* **2009**, *48*, 10988–10994.
[45] A. Ho, S. R. Schwarze, S. J. Mermelstein, G. Waksman, S. F. Dowdy, *Cancer Res.* **2001**, *61*, 474–477.
[46] S. Rickling, L. Ghizdavu, F. Pierard, P. Gerbaux, M. Surin, P. Murat, E. Defrancq, C. Moucheron, A. Kirsch-De Mesmaeker, *Chem. Eur. J.* **2010**, *16*, 3951–3961.
[47] A. D. MacKerell, N. Banavali, N. Foloppe, *Biopolymers* **2000**, *56*, 257–265.
[48] E. F. Pettersen, T. D. Goddard, C. C. Huang, G. S. Couch, D. M. Greenblatt, E. C. Meng, T. E. Ferrin, *J. Comput. Chem.* **2004**, *25*, 1605–1612.

Received: March 10, 2016
Published Online: April 27, 2016

